




# Analysis of the stabilising effect of ribs of reinforced sprayed concrete (RRS) in the Løren road tunnel

Are Håvard Høien<sup>1,2</sup>  · Bjørn Nilsen<sup>1</sup>

Received: 20 June 2017 / Accepted: 29 January 2018  
© The Author(s) 2018. This article is an open access publication

## Abstract

The Løren tunnel is a road tunnel at Ring road 3 in Oslo, Norway. The tunnel has a length of 915 m in rock, has two tubes with three lanes and breakdown fields, and was first opened in 2013. For rock support in the case of weak rock masses, ribs of reinforced sprayed concrete (RRS) were used. The scope of this article is to present and analyse the results of a measurement programme carried out on three of these ribs. This is done by focusing on deformations in the rock and the support function of the ribs due to these deformations. The instrumented RRS had strain meters installed in the reinforcement and the concrete. From the surface above the RRS, multipoint borehole extensometers were placed to survey the soil and rock mass deformations caused by tunnel advancement. In addition, 2D and 3D rock stress measurements and rock property testing were conducted. The measurements and numerical modelling show that the deformations are too small to cause a considerable load on the installed support construction and that the 2D stress measurements seem to best fit the in-situ stress conditions. The rock mass quality in the area of this study is on the verge of where one usually starts using reinforced ribs. It is concluded that the RRS are not required because of deformations in the rock but, rather, because of the need to lock blocks, increase the friction in joints and prevent movement in larger filled joints. For this purpose, the RRS should probably be designed differently to get the most out of the materials used.

**Keywords** Rock support · Ribs of reinforced sprayed concrete (RRS) · Displacement monitoring · Support design

## Introduction

To create stable and durable underground openings, reinforcement and support of the rock mass is required. The needed reinforcement and support vary greatly, from almost none in good-quality rock mass with favourable stress conditions to massive support in poor and swelling masses with unfavourable stress conditions.

The rock support in weak rock masses follows different traditions around the world. For instance, in the Alpine countries, rigid systems with deformable elements are common (Aksoy et al. 2012; Schwingenschloegl and Lehmann 2009),

while the Norwegian tradition is to use lean support, which improves the self-bearing capacity of the rock mass (Norsk Forening for Fjellsprengningsteknikk, NFF 2008).

The more rigid systems include steel beams with parts that deform at a certain load, together with rock bolts, reinforcing mesh and sprayed concrete between the beams (Barla et al. 2011). In Norway today, a system of rebar-reinforced ribs of sprayed concrete (RRS) is the preferred choice for rock support in weak and swelling rock mass. These RRS are used in combination with spiling bolts, radial rock bolts and sprayed concrete as an integrated part of the excavation process (NFF 2008). The current practice regarding the use of ribs is largely based on experience and empiricism.

The Norwegian Geotechnical Institute (NGI) and Norwegian University of Science and Technology (NTNU) have performed research related to the performance of RRS. The NGI has applied numerical modelling to develop dimensioning rules (Grimstad et al. 2002) and calculated loads based on the in-situ monitoring in the Finnfast road and Bærum railway tunnels (Grimstad et al. 2008). These dimensioning rules have been incorporated in the rock support chart of the

---

✉ Are Håvard Høien  
are.hoien@vegvesen.no

<sup>1</sup> Norwegian University of Science and Technology, Sem Sælands veg 1, 7491 Trondheim, Norway

<sup>2</sup> Norwegian Public Roads Administration, Postboks 8142 Dep, 0033 Oslo, Norway

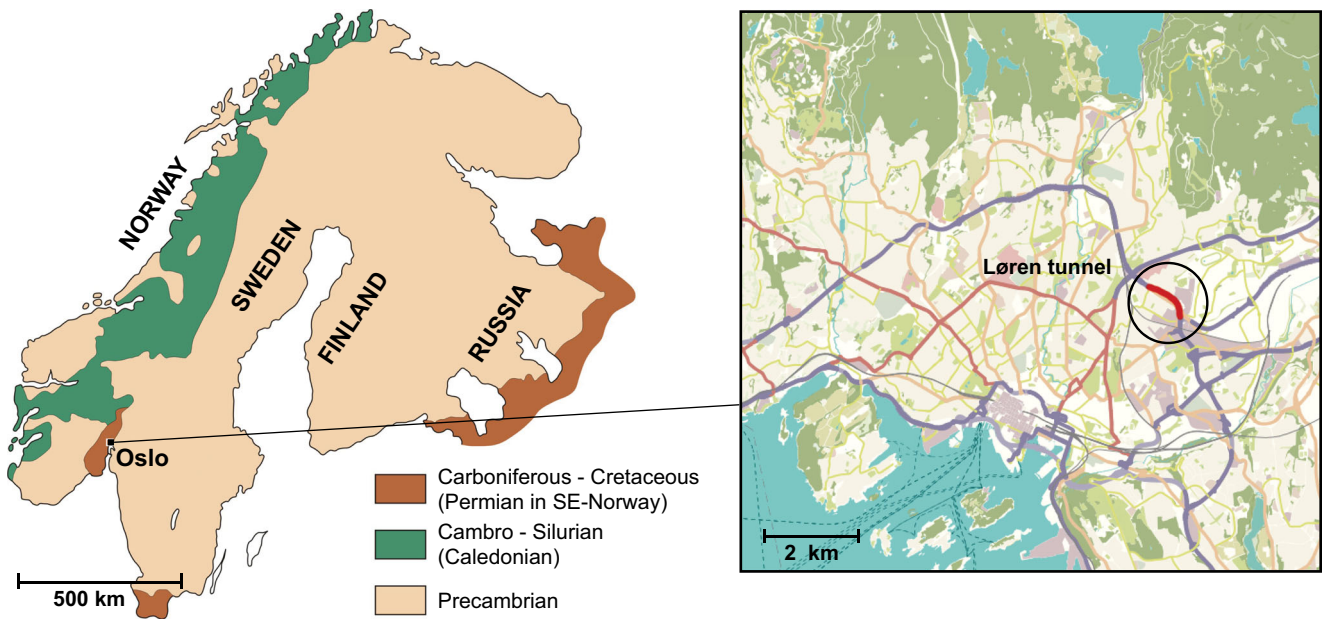


Fig. 1 Location of Oslo and the Løren tunnel in the Scandinavian regional geology

rock mass quality classification and support design system—the NGI Q-system (NGI 2013). The monitoring data from the Finnfast tunnel have also been studied at the NTNU by Mao et al. (2011), who used a 3D numerical model to analyse the loading effects of swelling rock on RRS.

However, to fully understand the mode of operation of the RRS concept, more monitoring, analysis and documentation are required. As a contribution to this, testing of rock mass properties and monitoring of the RRS at the Løren tunnel project have been done and will be described in this article.

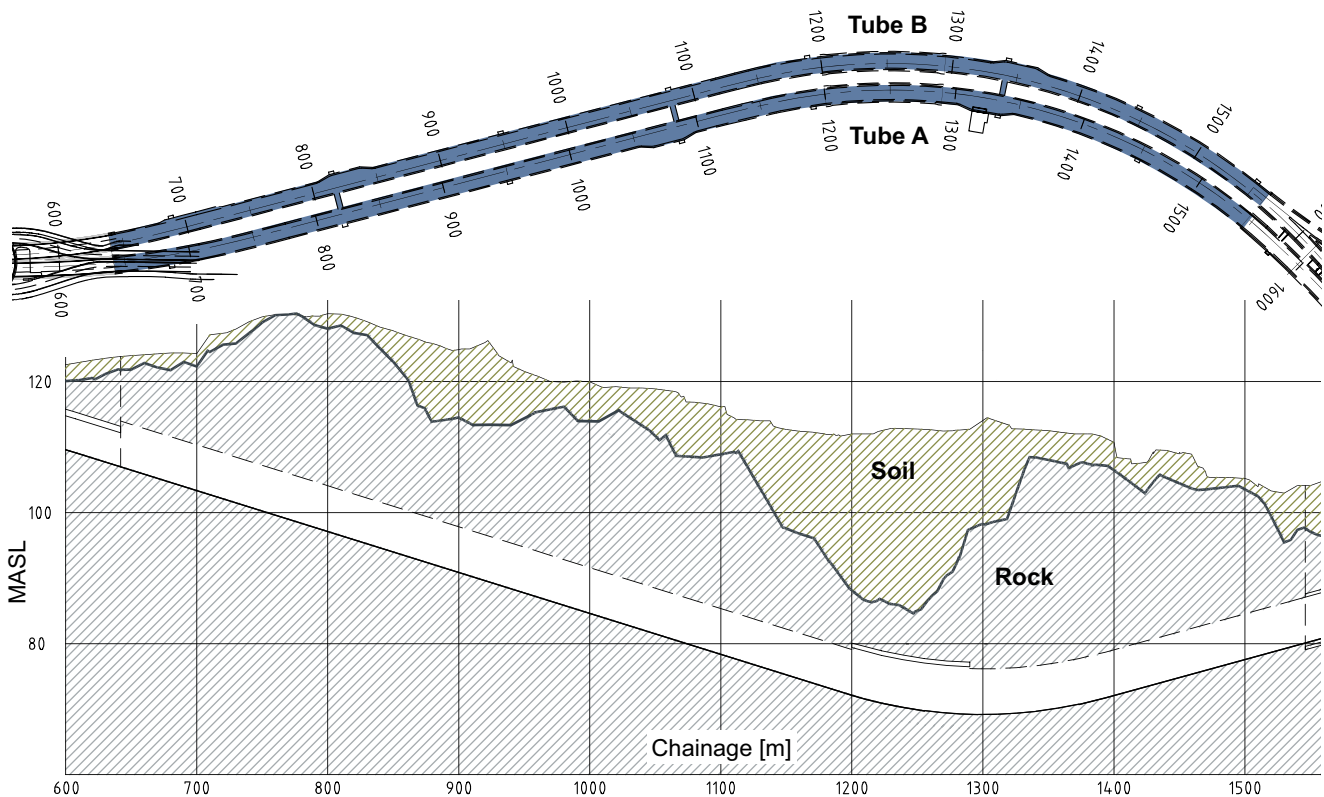
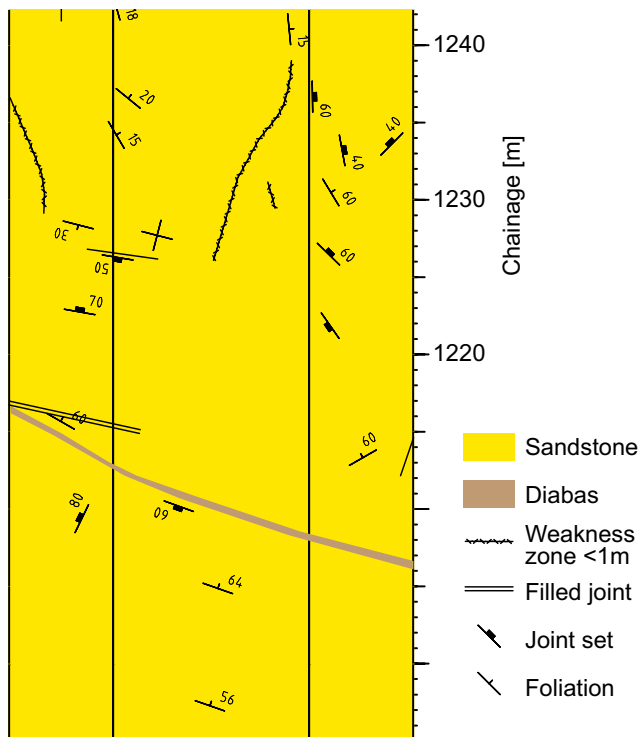


Fig. 2 Plan view and longitudinal profile of the Løren road tunnel



**Fig. 3** Geology of tube B, mapped during excavation. The map is drawn as a fold-out tunnel profile. For more details, see Høien and Nilsen (2014)

The results have been used as input in a two-step numerical analysis.

### Description of the Løren tunnel

The Løren tunnel is a 915-m road tunnel located in Oslo, Norway (see Fig. 1). The tunnel was excavated from one end by drilling and blasting technique and continuous grouting. It has two tubes with three lanes and emergency stop fields, which results in tunnel widths of 13–16 m and face areas of 105–135 m<sup>2</sup>. Tube B was excavated approximately 30 m ahead of tube A on descending profile numbers (see Fig. 2). Above the tunnel, there is a mix of residential and commercial buildings founded on soft, sensitive clay and sandy, gravelly soil with a thickness of up to 30 m. The tunnel opened for traffic in 2013.

During the excavation of the tunnel, its geology was mapped (Fig. 3) and a Q-value was estimated after each blast by an engineering geologist. The geological information was compiled in the tunnel documentation software Novapoint Tunnel (Vianova Systems 2011) using a fold-out tunnel profile (Humstad et al. 2012). A geological longitudinal section map, as shown in Fig. 4, was created based on this mapping and the pre-construction investigations. The rock types mapped in the tunnel were sandstones, calcareous shale, black shale, nodular limestone and intrusions of rhomb-porphry, diabase and syenite. The intrusive rock is of Carboniferous–Permian age and the folding is a result of the Caledonian orogeny. The Caledonian orogeny is found from Scotland to the Norwegian mainland and up to Svalbard. The folded rock was deposited during the Cambrian Period (Ofte Dahl 1981).

### Monitoring and testing methodologies

In the following, the methodology and layout for testing and monitoring in the Løren tunnel will be described. It should be noted that the methodology, including the setup of the extensometer and RRS monitoring, was very similar to that used in the Bærum and Finnfast tunnels (Grimstad et al. 2008), as referred to in the Introduction.

### Extensometers from the surface

Three Geokon multipoint borehole extensometers (MPBX), each with three groutable anchors, were installed from the surface by the NGL, which also provided the resulting monitoring data (see Fig. 5). At chainage 1220, one extensometer was installed above each tunnel tube, and at chainage 1030, one extensometer was installed above tube B. Table 1 shows the depths of the anchors. Anchor 1 was intended to be placed in the rock just beneath the soil/rock transition. Anchor 3 was placed just above the tunnel roof. As an example, the extensometer setup and the setup for rib measurement described in the next section are shown for B1220 in Fig. 6.

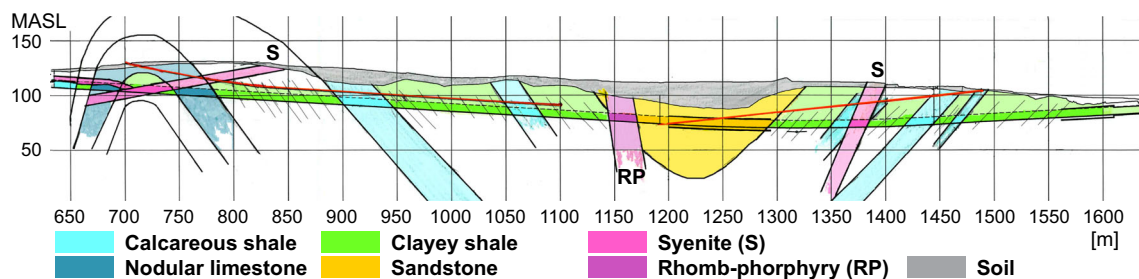


**Fig. 4** Longitudinal profile illustrating the rock type distributions and structural geology (Iversen 2011)

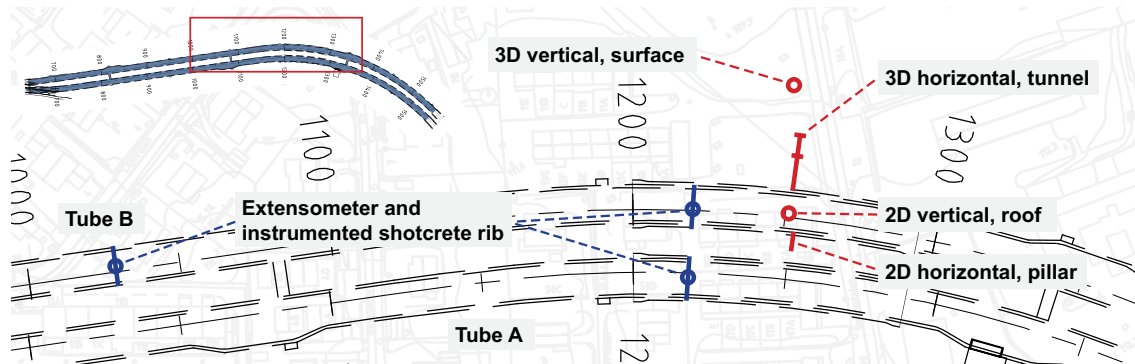


Fig. 5 Locations of extensometers, instrumented ribs of reinforced sprayed concrete (RRS) and rock stress measurements

At the surface, the extensometer had a metal head with three holes for measuring deformations. The measurements were conducted with a clock-gauge caliper, which was calibrated before and after each extensometer reading. Three measurements were performed for each anchor and an average of the three values was used in the resulting graphs.

### Monitoring of the RRS

To measure the load on the ribs, instruments were mounted on the rebar before sprayed concrete was applied (see Fig. 7). The rebar in the rib was 20 mm in diameter and placed with a centre-to-centre (c/c) spacing of approximately 100 mm. One concrete strain meter and one rebar strain meter were placed in pairs at five locations along the tunnel profile, as illustrated in Fig. 6. Both instruments used vibrating wires to measure the strain and had a built-in gauge for temperature correction. The stresses for the steel were calculated from the monitored strain based on using a deformation modulus of 200 GPa.

In the Finnfast and Bærum tunnels, pressure cells were installed in an attempt to measure the support pressure and ring pressure in the RRS. This was discarded in this case because of the unreliable results experienced at Finnfast and Bærum (Grimstad et al. 2008) and problems with applying the sprayed concrete without creating cavities. If larger deformations and loads are expected and the cells are sprayed before the mounting of the rebars in the RRS, such instrumentation will likely provide very interesting data.

Table 1 Anchor depths (depth below surface) for the extensometers

	B1220	A1220	B1030
Soil/rock	22.5 m	26 m	7.5 m
Anchor 1	24 m	28 m	18 m
Anchor 2	29 m	32 m	23 m
Anchor 3	30 m	33 m	24 m

### Rock stress measurements

In-situ stresses have been measured based on three principles: 2D doorstopper overcoring in the pillar and roof, 3D overcoring inside the tunnel and 3D overcoring from the surface. The locations of the different measurement holes are shown in Fig. 5.

Overcoring measurement is performed by drilling a hole, gluing strain gauges to its walls and then overcoring this first hole with the strain gauges inside. The strain from the expansion of the rock is then used, together with the material parameters, to calculate the stress to which the rock was originally exposed (Kim and Franklin 1987). The stress measurements from the surface were performed by Pöyry SwedPower

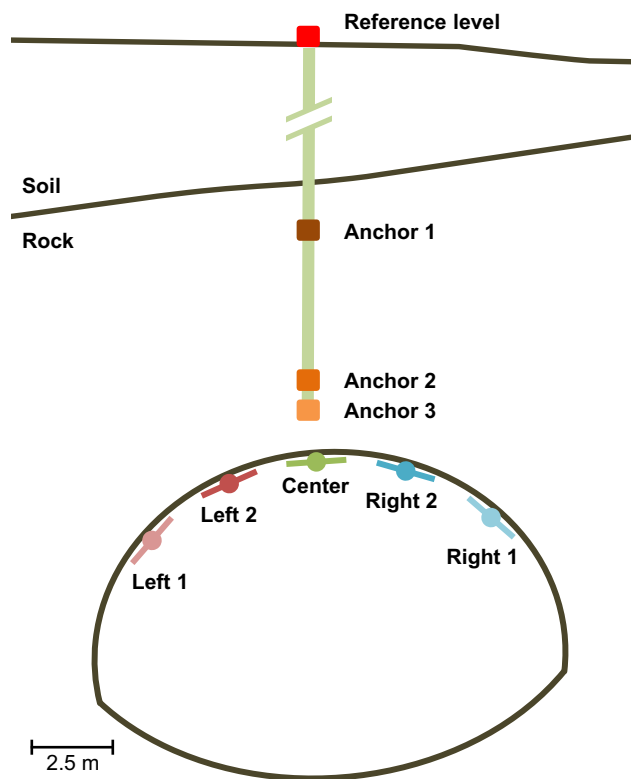
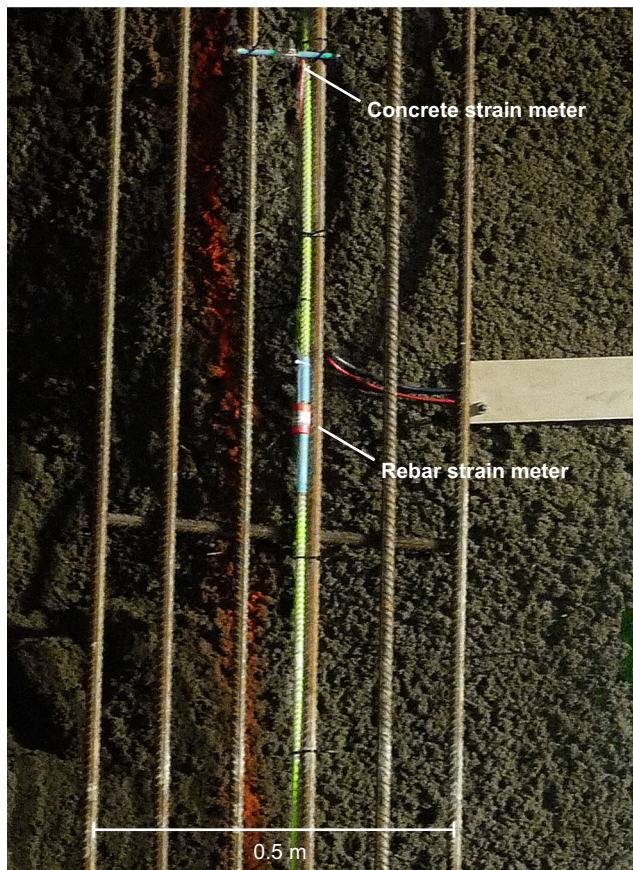


Fig. 6 Extensometer and strain measurement setup at chainage B1220



**Fig. 7** Concrete and rebar strain meters mounted on the rib before the application of sprayed concrete

AB, and those from the tunnel were performed by SINTEF. For more information about the specific methods used, reference is made to Sjöberg and Klasson (2003) and Larsen and Trinh (2014), respectively.

For the surface measurement, an 86-m hole was drilled. An attempt was made to measure at depths of 58.9, 60.6 and 65.3 m, but due to there being too many joints, no measurements were successful.

The 3D measurements in the tunnel were performed between 12.5 and 18 m from the tunnel wall, and five of these

measurements were successful. The software program DISO (Determination of In-situ Stress by Overcoring) was used to calculate the stress and validate the measurements (Larsen 2010).

The 2D doorstopper overcoring was also carried out by SINTEF. This method provides the stress for the plane perpendicular to the borehole and can be used for measurements up to 10 m from the tunnel contour. One measuring series usually consists of seven to ten measurements and requires about 1.5 days to complete (Larsen and Trinh 2014). Based on this method, five measurements were performed in the tunnel roof at 1–3.5 m into the borehole, and seven measurements were performed in the pillar at 0.8–4.1 m into the borehole (Larsen 2010).

## Results of testing and monitoring during tunnelling

### Rock mass properties

The rock mass parameters based on the testing of samples from holes for rock stress measurement and core drilling are presented in Table 2. There are generally four types of rock in the area: sandstone, syenite, rhomb-porphry and diabase. Sandstone normally has a lower strength than the other rocks, which are intrusive. Considering the strength values and geological mapping, the 3D stress measurements were performed in syenite and the 2D measurements were performed in sandstone. The rock from the core hole is described in the core log (Haug et al. 2007) as sandstone for chainages 1010–1012 and shale for chainages 1217–1223.

For the cores related to 3D stress measurement, point load tests were also performed, indicating a compressive strength of 221 MPa and a tensile strength of 13 MPa. The large variations seen in some of the values in Table 2 may be due to anisotropy caused by testing parallel with the folded but still visible bedding planes (CH 1010–1012 and 2D hsm) and petrographic variations (3D sm).

**Table 2** Material parameters for the rock from the core hole (CH), the hole for 3D stress measurement (3D sm), the hole for 2D horizontal stress measurement in the pillar (2D hsm) and the hole for 2D vertical stress measurement in the tunnel roof (2D vsm)

	Rock type	UCS (MPa)	No.	E-modulus (GPa)	No.	Poisson's ratio	No.	Density (kg/m <sup>3</sup> )	No.
CH 1010–1012	Shale	na <sup>b</sup>	4	37.6	2	0.170	1	2741 ± 17.3	4
CH 1217–1223	Sandstone	80.6 ± 16.0	4	42.6 ± 17.2	4	0.155 ± 0.013	4	2753 ± 208.9	4
3D sm	Sandstone/syenite <sup>a</sup>	146.1 ± 45.89	4	56.0 ± 10.56	4	0.185 ± 0.051	4	2795 ± 161.8	4
2D hsm	Sandstone	62.2	2	44.8 ± 14.57	4	0.120	2	2682	2
2D vsm	Sandstone	29.0	2	37.0	2	0.210	1	2693	2

<sup>a</sup> Exact rock type not recorded

<sup>b</sup> Not given due to inconsistent testing values

**Table 3** Rock mass quality from mapping during tunnel excavation. The rock type is sandstone with a thin diabase dyke crossing between chainages 1200 and 1215

From chainage	To chainage	Rock class	Q-value	RQD	J <sub>n</sub>	J <sub>r</sub>	J <sub>a</sub>	J <sub>w</sub>	SRF
A1204	A1208	D	1.2	50	6	1.5	4	1	2.5
A1208	A1211	D	3.1	62.5	6	1.5	2	1	2.5
A1210	A1215	D	1.2	50	6	1.5	4	1	2.5
A1215	A1219	E	0.56	45	12	1.5	4	1	2.5
A1219	A1222	D	2.5	50	6	1.5	2	1	2.5
A1222	A1225	D	3.1	62.5	6	1.5	2	1	2.5
A1225	A1228	D	1	60	12	1.5	3	1	2.5
A1228	A1208	E	0.83	50	12	1.5	3	1	2.5
B1203	B1210	D	1.6	70	6	1	3	1	2.5
B1210	B1214	C	4.1	82.5	6	1.5	2	1	2.5
B1214	B1219	C	7.8	62.5	4	1.5	2	1	1.5
B1219	B1222	D	1	62.5	12	1	2	1	2.5
B1222	B1226	E	0.16	37.5	12	0.5	4	1	2.5
B1226	B1229	E	0.62	50	12	1.5	4	1	2.5
B1229	B1232	E	0.42	50	12	1	4	1	2.5

The rock mass quality based on mapping during excavation and core logging is presented in Tables 3 and 4. As shown, the resulting Q-values range from fair (C) to very poor (E). The difference in RQD values between the tunnel mapping and the core mapping is likely primarily due to blast damage and the angle between the core hole and the joint sets. In the further use of these data in the numerical model, great emphasis has been placed on selecting values that are representative of the rock mass of the respective area as a whole.

### Displacements monitored by extensometers

The results of the displacement monitoring are shown in Figs. 8, 9 and 10, with values above 0 (black font) indicating upward movement and values below 0 (red font in parentheses) indicating downward movement in millimetres. Because of an uplift of the terrain between 1 and 2 cm, which was caused by the rock mass grouting, the values had to be corrected for the movement of the head of the extensometer before identifying the deformations caused by the advancement of the tunnel faces. The displacement of the head in the figures is shown as the “Reference level”.

**Table 4** Rock mass quality from the logging of cores from probe drilling (Iversen and Kveen 2007). The core hole is sub-horizontal, and the rock and soil cover is approximately 70 m at these chainages, which places it close to the sole of the tunnel. The rock type is sandstone

From chainage	To chainage	Rock class	Q-value	RQD	J <sub>n</sub>	J <sub>r</sub>	J <sub>a</sub>	J <sub>w</sub>	SRF
1217	1218	B	198	90	3	2	2	0.66	1
1218	1219	B	20.9	95	3	2	2	0.66	1
1219	1220	B	13.33	80	3	2	2	0.5	1
1220	1221	B	14.17	85	3	2	2	0.5	1
1221	1222	B	16.67	100	3	2	2	0.5	1
1222	1223	B	17.6	80	3	2	2	0.66	1
1223	1224	B	19.8	90	3	2	2	0.66	1

In the charts, the distance from the MPBX is that from the far end of the holes. For B1220 and A1220, all grouting holes that may have influenced the rock mass in the area of the extensometers have a length of 15 m, with the packer placed 3 m into the hole, and a planned end pressure of 60 bar. For more details regarding the rock mass grouting, see Høien and Nilsen (2014).

### MPBX B1220

Tunnelling past the extensometer took place between 04.03.2010 and 17.03.2010, and the four observations made during this period were probably not influenced by the rock mass grouting. The readings are presented in Fig. 8. On 04.03.2010, the face was at chainage B1221.

In this period, a small rise can be observed from the first observation to the second observation. From this highest point to the fourth point, anchor 3 has been lowered 2.39 mm. At the fourth point, the tunnel has passed the extensometer by 20 m. The relative expansion between anchors 1 and 3 during the period is 1.61 mm.

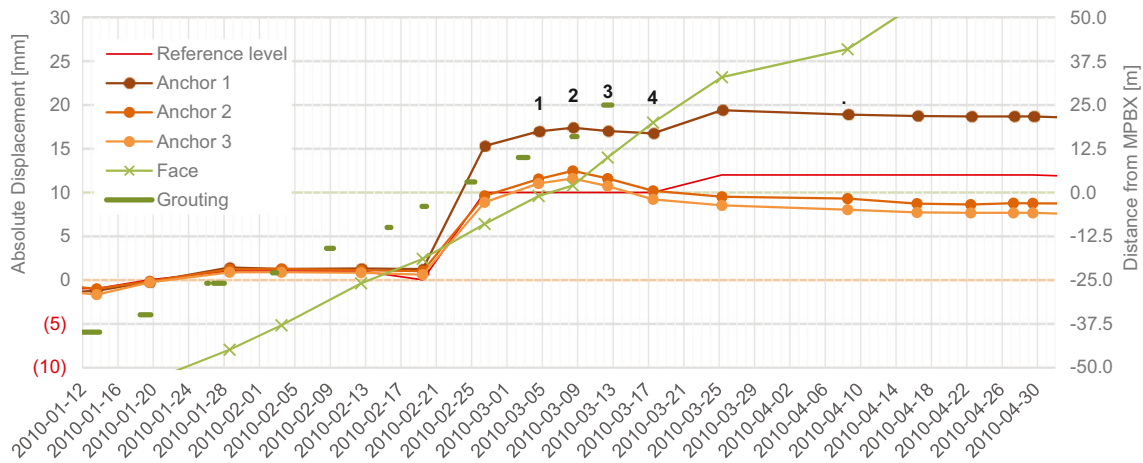


Fig. 8 Absolute displacement for the extensometer in tube B at chainage B1220. The numbers are the observations mentioned in the text

Between 17.03.2010 and 25.03.2010, for anchor 1, a lift of several millimetres can be observed. This corresponds to the dates for the rock mass grouting of tube A.

**MPBX A1220**

Tunnelling past the extensometer took place from 25.03.2010 to 22.04.2010. The first of the four observations during the period may have been influenced by the rock mass grouting performed on 26.03.2010. Two blast rounds were performed between the first and second observations and, because of this, there might have been a small peak if more measurements had been carried out.

From 08.04.2010 (observation 2) to 22.04.2010 (observation 4), there was a lowering of anchor 3 by 2.16 mm, and the face was 25 m past the extensometer. Note that the line for anchor 3 is above that for anchor 2 in the figure. The relative expansion between anchors 1 and 3 during this period was 2.07 mm.

**MPBX B1030**

Tunnelling past the extensometer, at chainages B1039 to B1011, was carried out from 01.07.2010 to 10.08.2010. During this period, there was a stop at A1030 for 3–4 weeks due to summer vacation. The excavation of chainages A1030 to A1027 was carried out on 03.08.2010. Before this blast round, an extra grouting cycle with 15-m holes was conducted. In addition, anchor 3 was exposed and broken during blasting. It is, therefore, not possible to determine whether any deformation occurred during the tunnelling towards the extensometer, and only minor deformations were recorded after the tunnel passed.

**Strain measurements in the RRS**

The strain measurements for the rebar are presented in Figs. 11, 12 and 13. In the figures, 100 μS is equal to 20 MPa in the steel, which, again, gives a load of 6.3 kN in the rebar.

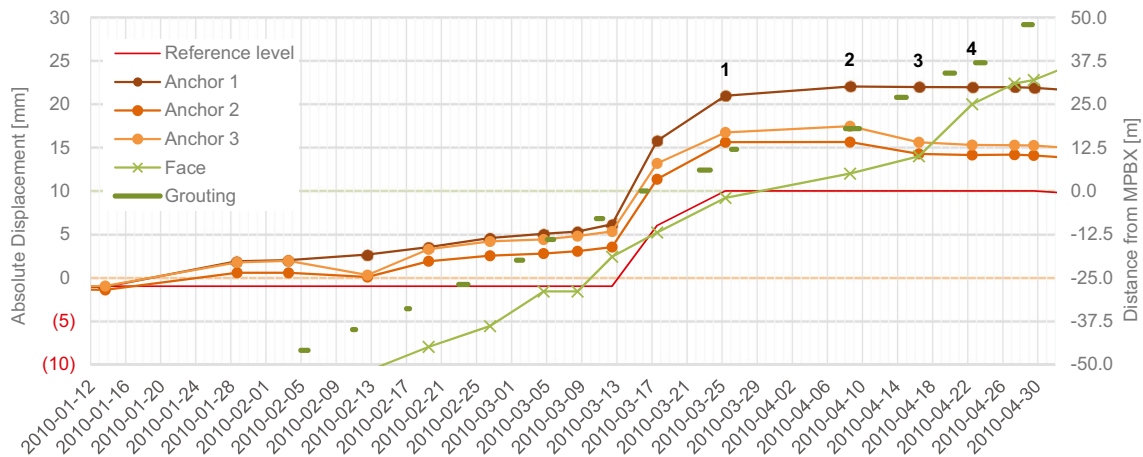


Fig. 9 Absolute displacement for the extensometer in tube A at chainage A1220. The numbers are the observations mentioned in the text

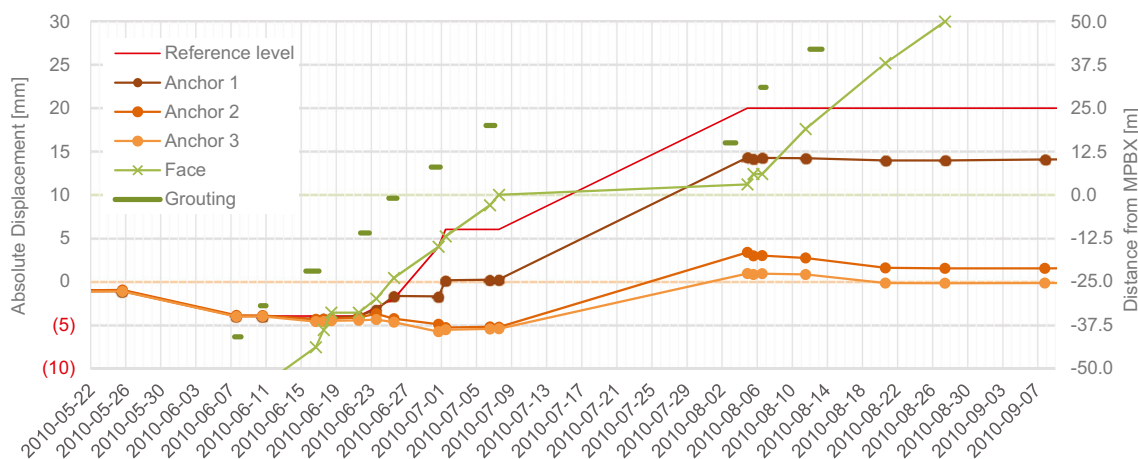


Fig. 10 Absolute displacement for the extensometer in tube B at chainage B1030. The numbers are observations mentioned in the text

Negative values are compression and positive values are tension. The rebar in the ribs is Ø20 mm B500NC, which has a yield strength of 500 MPa. The position of the strain gauges is shown in Fig. 6.

According to Pedersen et al. (2010), sprayed concrete has a drying shrinkage of 0.8–1.2 ‰. Related to Figs. 11, 12 and 13, this corresponds to – 800 to – 1200 µS. The drying shrinkage is time-dependent and dependent on the relative humidity (Standard Norge 2008). Due to uncertainty regarding the size of the shrinkage, the data in the figures are not corrected for this. For a tunnel with a width of 10 m, a drying shrinkage of 1.0 ‰ for an unrestrained arch will give a reduction in diameter of approximately 10 mm. Because the rebar is embedded in and coupled to the concrete through a chemical and mechanical bond, the stiffness of the rebar will create a force that counteracts the concrete shrinkage, which results in a

strain in the rebar and the cracking of the concrete. Rebar strain from concrete shrinkage will be negative where it is embedded in concrete and positive in and close to the cracks (Gilbert 2001). Other restraints from, e.g. bolts and irregular rock surfaces will also reduce the drying shrinkage.

### Rock stress measurements

The measured stresses are generally much higher than what is induced by gravity. This is, however, as expected in this region and, according to Myrvang (2001), this may be caused by folding of the rock, erosion of overlaying rock masses and/or plate tectonics. Myrvang also states that the cooling of igneous rock may create local compressive and tension stresses in the rock mass.

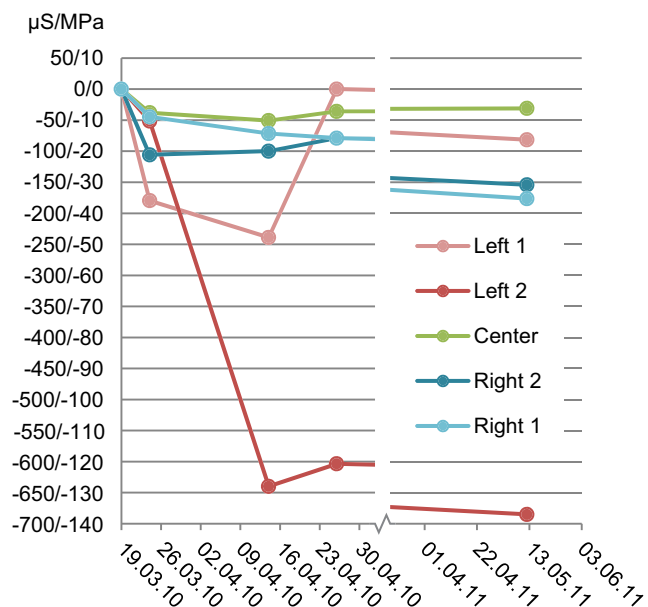


Fig. 11 Rebar strain in the RRS at B1220

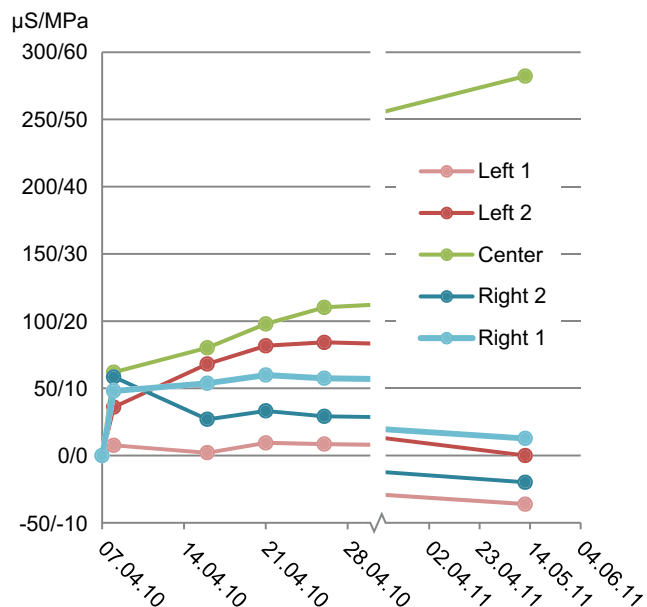


Fig. 12 Rebar strain in the RRS at A1220



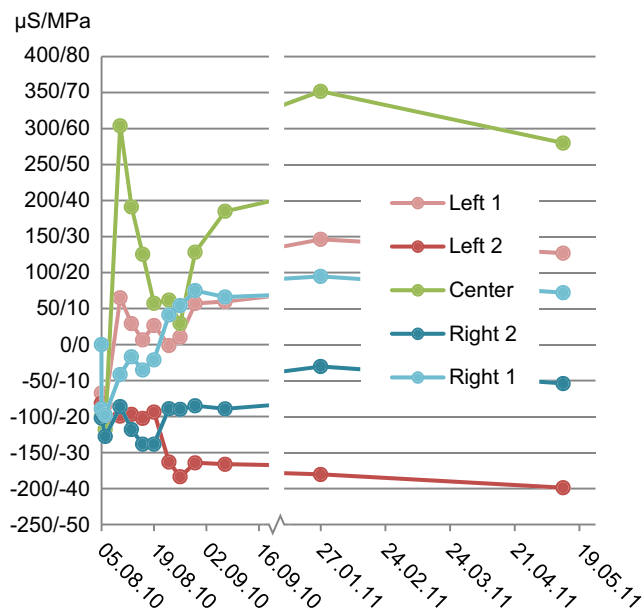


Fig. 13 Rebar strain in the RRS at B1028

### 3D overcoring

The results of the 3D overcoring carried out by SINTEF (Larsen 2010) show that the major principal stress is 13.6 MPa, horizontal and perpendicular to the tunnel axis. The minor principal stress is 2.2 MPa, with an orientation parallel to the tunnel axis and a 43° dip to the NW. Both have a margin of error of approximately ± 3 MPa. For more details, see Fig. 14 and Table 5. The test report states that there are substantial tectonic/geologic stresses in the area and that these stresses are at a level that may cause stress-induced cracks (Larsen 2010).

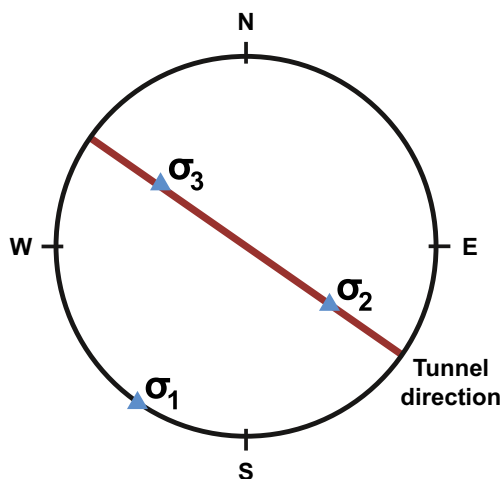


Fig. 14 Pole plot showing the directions of principal stresses based on 3D stress measurements in the tunnel wall (Larsen 2010). (Equal area projection, lower hemisphere)

### 2D overcoring

The stresses measured in the pillar and the tunnel roof are presented in Tables 6 and 7, respectively. Tunnel geometry control scanning showed that the width of the pillar in this area was slightly above 7 m.

The pillar hole was drilled halfway through and had a peak at about 3 m into the hole before beginning to decrease towards the middle. Theoretically, the stress should be highest at the pillar wall and decrease towards the middle. According to Myrvang (2001), fracturing from blasting in the pillar wall will move the stress peak towards the middle, as was observed in this case, and this is probably the reason for the discrepancy. As for the pillar hole, the roof hole showed increasing stresses from the contour.

As seen in Tables 6 and 7, the stresses vary quite a bit, which may be because the hole is perpendicular to the bedding.

### Numerical modelling

To evaluate the measured data and the installed rock support, two-step numerical modelling has been performed. In the first step, the stress measurements are evaluated using two stress configurations (SC1 and SC2). As a second step, the most probable stresses found in the first step are used to investigate loads on and deformations of the RRS.

The 2D finite element software program RS<sup>2</sup> (also known as Phase2 9.0) was used (Rocscience Inc. 2016).

### Model description

Numerical modelling was carried out for the cross-section at chainage 1220 (see Fig. 15). The geometry of the model is based on topographical data, borehole data, plan drawings and tunnel scanning. The tunnel profile has been extended by 1 m relative to the theoretical blasting profile to fit the real geometry as shown by the scanning data.

The boundary conditions are open at the top, restrained in the *x* direction at the sides and fixed at the bottom. Before the tunnel is “excavated”, the model has a reference stage to zero out the deformations due to the settling of the model.

The constitutive models used are Mohr–Coulomb and Generalised Hoek–Brown for the soil and rock, respectively.

To simulate the blast damage zone, the model includes three 0.3-m-thick “rings” around the tunnel tubes, with an increasing amount of blast damage towards the tunnel periphery (see Table 9), resulting in a blast damage zone of 0.9 m.

**Table 5** Stresses from 3D stress measurements performed in the tunnel wall (Larsen 2010)

	Stress (MPa)	Global direction	Direction relative to tunnel
$\sigma_1$	13.6 ± 2.8	215.5/0	89.5
$\sigma_2$	5.0 ± 1.3	124/47	359
$\sigma_3$	2.2 ± 3.2	307/43	178
$\sigma_v$	3.70		
$\sigma_h$ (min)	3.46	125.7	
$\sigma_h$ (max)	13.54	35.7	
Tunnel		125	

### Input parameters for rock mass and soil

As input parameters for the rock mass, data from core hole logging and continuous geological mapping during the tunnel excavation were used. All rock testing was performed according to the International Society for Rock Mechanics (ISRM) suggested methods (ISRM 2007). For the core drilling, data from chainages 1217–1223 and the 2D doorstopper stress measurement (see the rock mass properties section of Table 2) were used to calculate the mean. The Q-value parameters were determined mainly based on the tunnel mapping (see the rock mass properties section of Tables 3 and 4). These data were then used to calculate the rock mass properties in RocData (Rocscience Inc. 2015) by adjusting for rock mass quality based on the Geological Strength Index (GSI) and blast damage. The GSI was not systematically mapped in the tunnel (like Q-values) and, therefore, it has been calculated from RQD,  $J_r$  and  $J_a$  using the following equation (Hoek et al. 2013):

$$GSI = \frac{52 J_r / J_a}{(1 + J_r / J_a)} + RQD / 2 \quad (1)$$

Tunnel blasting was performed with a reduced charge at the perimeter and the second row, but substantial damage to the tunnel contour was still registered. To include the effect of blast damage on the rock, the material parameters for

**Table 6** Stress measurements in the pillar.  $\sigma_1$  and  $\sigma_2$  are the principal stresses in a vertical plane along the pillar

Hole depth (m)	$\sigma_1$ (MPa)	$\sigma_2$ (MPa)	Direction from vertical (°)
0.8	1.1	− 0.9	16
1	0.3	− 0.9	10
2.5	7.6	− 3.4	22
2.8	6.1	− 0.4	1
3.2	7.7	0.7	− 15
3.7	2	− 1.2	− 77
4.1	2	− 0.6	44

sandstone have been calculated with D-values of 0, 0.2, 0.4 and 0.6 (Hoek and Diederichs 2006).

The Q-value for the sandstone in the area is 1.4; ( $RQD / J_n$ ) \* ( $J_r / J_a$ ) \* ( $J_w / SRF$ ) = (65/9) \* (1.5/3) \* (1/2.5)), which gives a GSI of 50 using Eq. 1. For the soil and sandstone, Poisson's ratios of 0.2 and 0.14 gives vertical/horizontal stress ratios of 0.25 and 0.16 for gravity-driven stresses, respectively.

For the soil, which consists of clay, silt and some sand, input parameters have been selected based on the log from the drilling of the holes for the extensometers.

The materials in the model are elastic, and the properties of the soil and sandstone are shown in Tables 8 and 9.

### Rock stresses

As input for the in-situ stresses, two models were used based on the available data. Both include vertical and horizontal gravity-driven stresses, with the vertical component being based on soil and rock load, and the horizontal component being derived from applying the Poisson value to the vertical component. For the rock, an additional horizontal component is also included to simulate tectonic or other remnant stresses.

The first model, stress configuration 1 (SC1), is based on the results of the 3D stress measurements, where the additional horizontal stresses are set as the measured data,  $\sigma_{h \text{ (max)}}$  is 13.54 and  $\sigma_{h \text{ (min)}}$  is 3.46. The direction of the major horizontal stress corresponds to the in-plane stress, and the minor horizontal stress corresponds to the out-of-plane stress in the model.

In the second model, stress configuration 2 (SC2), the additional horizontal stress was varied between 1.00 and 2.75 MPa in steps of 0.25 MPa. The resulting stresses in the model corresponding to the 2D stress measurement boreholes were exported for each step and plotted in a graph, together with the measured data, to find the additional horizontal stress that best fits.

For both models, the gravitational stresses are given by the density of the material and Poisson's ratio. This provides horizontal/vertical stress ratios for the soil and sandstone of 0.25 and 0.16, respectively. The gravitational stress contribution is, thus, approximately 1.0 MPa vertically and 0.2 MPa horizontally at the height of the tunnel floor.

### Loading effects on RRS

To analyse the loading from rock deformations on the rock support, the most likely rock stress distribution based on the first step of the analysis was used in a new model. The installation of the support took place at the same stage as the excavation of the tunnel, resulting in the concentration of the total load on the support. This will theoretically give a higher load

**Table 7** Stress measurements in the tunnel roof.  $\sigma_1$  and  $\sigma_2$  are the principal stresses in a horizontal plane above the tunnel roof

Hole depth (m)	$\sigma_1$ (MPa)	$\sigma_2$ (MPa)	Global direction (°)	Direction relative to tunnel (°)
1	2.2	-0.5	66	121
1.4	4.1	0.7	75	130
1.8	2	0.2	53	108
3	3.5	1.5	147	202
3.5	0.7	-3	74	129

as compared to reality because some of the deformations will occur before installation (Hoek 1998).

The tunnels in the modelled area were supported with grouted and pre-stressed bolts (c/c 1.5 m), fibre-reinforced sprayed concrete (thickness 0.18 m), spiling bolts (c/c 0.3 m) and RRS (c/c 2.5 m) with six rebars that were 20 mm in diameter at a c/c of 0.1 m. The rebar was pre-bent and held in place by mounting bolts, not rock bolts, as are typically used, to follow the theoretical profile (see Fig. 16). The thickness of the ribs was between approximately 0.3 and 0.5 m, and their width was about 0.7 m. The sprayed concrete layer used to smooth out the blasted profile, where the ribs were used, was often considerably thicker than the prescribed 0.18 m due to overbreak.

In the numerical model, the support has been simplified by modelling the rib and sprayed concrete as reinforced cast concrete. The simplification involved the division of the number of rebars and the amount of concrete used in a rib by 2.5 (the c/c distance) to distribute it on the 1-m unit distance in the 2D model. Based on this, the rib and reinforced sprayed concrete

were modelled as 0.3-m-thick double-reinforced cast concrete with  $\text{Ø}20$  mm rebar at a 0.4-m spacing.

This “cast concrete” is modelled as fully bonded with the rock because the displacement measurements show only small movements, which should not detach the concrete from the rock. The rebar has a tensile strength of 400 MPa, and the concrete has a deformation modulus of 25,000 MPa and a compressive strength of 40 MPa. In addition, grouted and pre-stressed  $\text{Ø}20$ -mm bolts with a length of 4 m, a c/c of 1.5 m in and out of plane, and a strength of 157 kN were included in the analysis. A summary of the support is presented in Table 10.

## Results of numerical modelling

### Stress configuration 1 (SC1)

When applying the results from the 3D stress measurement, the model has an additional in-plane horizontal stress of

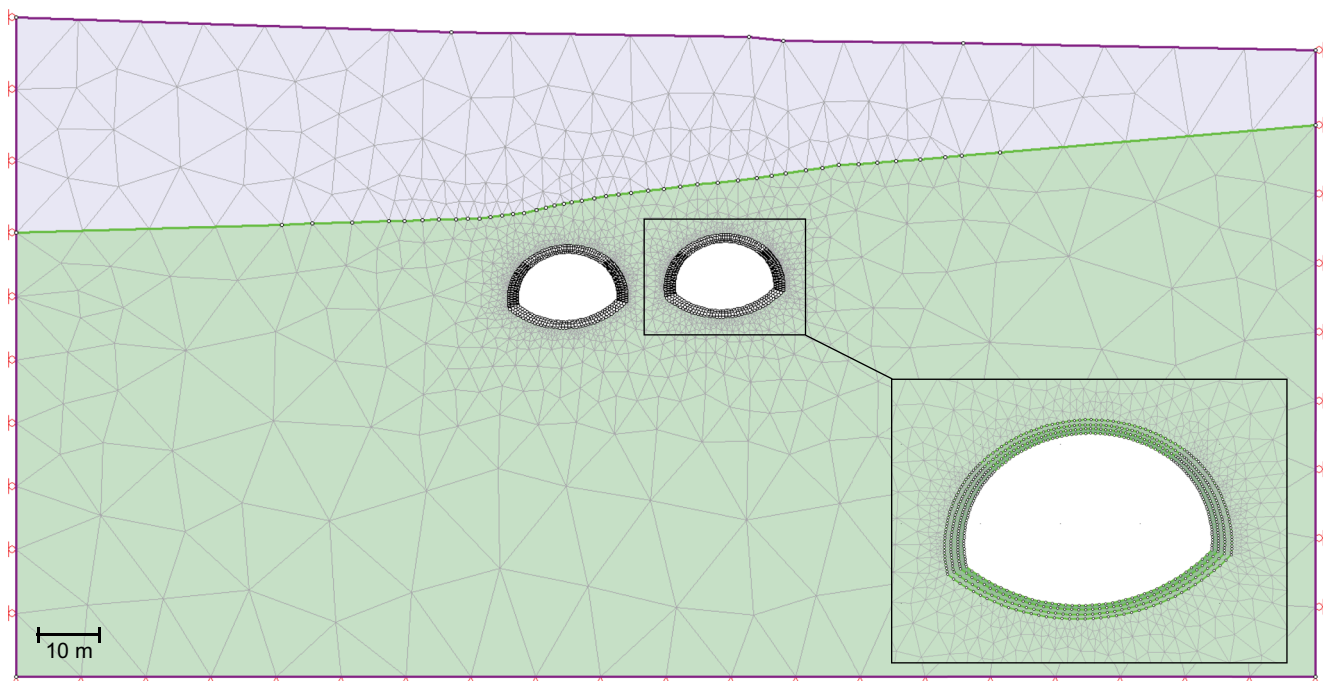


**Fig. 15** Geometry of the numerical model for chainage 1220. Purple is soil and green is rock (sandstone)

**Table 8** Material properties of the soil

Density (MN/m <sup>3</sup> )	0.02
E-modulus (MPa)	30
Tensile strength (MPa)	0
Friction angle (°)	33
Cohesion (kPa)	1
Poisson's ratio	0.2

13.6 MPa. As seen in Fig. 17, this results in very high stresses (exceeding 25 MPa) in the roof and, as seen in Fig. 18, negative minor principal stresses in the walls.

### Stress configuration 2 (SC2)

The major principal stresses ( $\sigma_1$ ) exported from the models for the various additional horizontal stresses are presented, together with the results of the 2D measurement in the roof and pillar, in Figs. 19 and 20. The exported values correspond to the placement of the roof and pillar measurement holes. In the tunnel roof, the direction of  $\sigma_1$  is tangential to the tunnel periphery and gradually begins to follow the soil/rock surface with decreasing depth, while in the pillar, this direction is vertical. By comparing the median values for the depth range of 1–3.5 m to the roof data, an additional horizontal stress of 1.50 MPa was found to give the best fit with the measurements. The distribution of the major and minor principal stresses for an additional horizontal stress of 1.50 MPa is presented in Figs. 21 and 22, respectively.

### Performance of the RRS

As concluded above, the model providing the results that best correspond with the measured data is that with an additional horizontal stress of 1.50 MPa. This model is, therefore, selected for further analysis.

**Table 9** Material properties of the sandstone

Blast damage (D)	0	0.2	0.4	0.6
Q-value	1.4	1.4	1.4	1.4
GSI	50	50	50	50
$\sigma_c$ intact (MPa)	61	61	61	61
Intact E-modulus (GPa)	42	42	42	42
Poisson's ratio	0.14	0.14	0.14	0.14
mi	17	17	17	17
Density (MN/m <sup>3</sup> )	0.027	0.027	0.027	0.027
Rock mass E-modulus (GPa)	12.9	9.7	7.2	5.3
mb	2.851	2.338	1.824	1.326
s	0.004	0.003	0.002	0.001
a	0.506	0.507	0.508	0.509

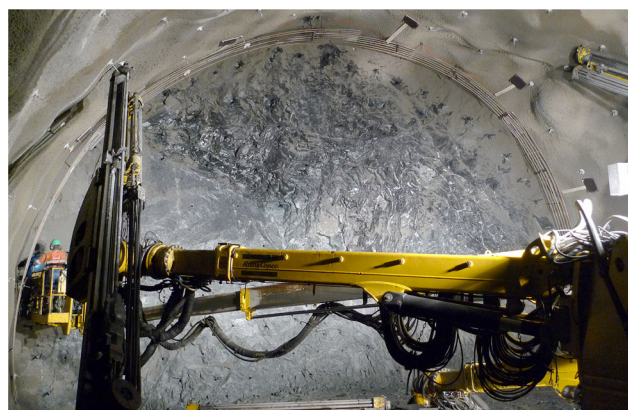


**Fig. 16** Ready-mounted rebar for the application of sprayed concrete. The light and dark plywood plates serve as protection for the instrumentation wiring during sprayed concrete application. The tunnel width is 15.5 m (the tunnel profile was extended to make room for the RRS)

The deformations in the model are shown in Fig. 23. The deformation downward in the tunnel roof is about 1 mm, and the relative expansion in the rock body is 0.12 mm. The corresponding displacement in the MPBX at B1220 is 2.39 mm and the relative expansion is 1.61 mm.

Figure 24 shows the capacity plot of the support. It illustrates that the deformations from the excavation generate only minor loads in the support construction compared to its capacity, with a safety factor above 10. The compression load in the rebar is 8–22 kN, which, in  $\mu\text{S}$ , is  $-130$  to  $-350$ . The capacity plots are based on Carranza-Torres and Diederichs's envelope principle (Carranza-Torres and Diederichs 2009), and show thrust versus moment and thrust versus shear plots for both the concrete and the reinforcement. Each beam (cast concrete) element along the tunnel periphery is plotted in the diagrams with its given values.

### Discussion and conclusions

The measurement programme described in this paper was designed to obtain data on the rock deformations caused by tunnelling as a basis for evaluating what loads this would give on the rock support.

The rock mass grouting has, to a large degree, disturbed the extensometer deformation measurements. The least-affected extensometer, at B1220, registered a deformation of 3.07 mm, which is expected to be related to the tunnel. This deformation occurred during the excavation from 1 m before the extensometer to 20 m after. According to Hoek et al. (1997), deformation begins about half a tunnel diameter before the measurement point, and about one-third of the total deformation is expected to have taken place when the tunnel reaches the measuring point. All deformations are expected to have taken place when the excavation has passed the

**Table 10** Actual and simplified/ equivalent support for the area around chainage 1220 for use in the numerical model.

<sup>a</sup>Calculation: (RRS thickness \* RRS width)/RRS distance + smoothing layer = (0.4\* 0.7)/ 2.5 + 0.18 ≈ 0.3

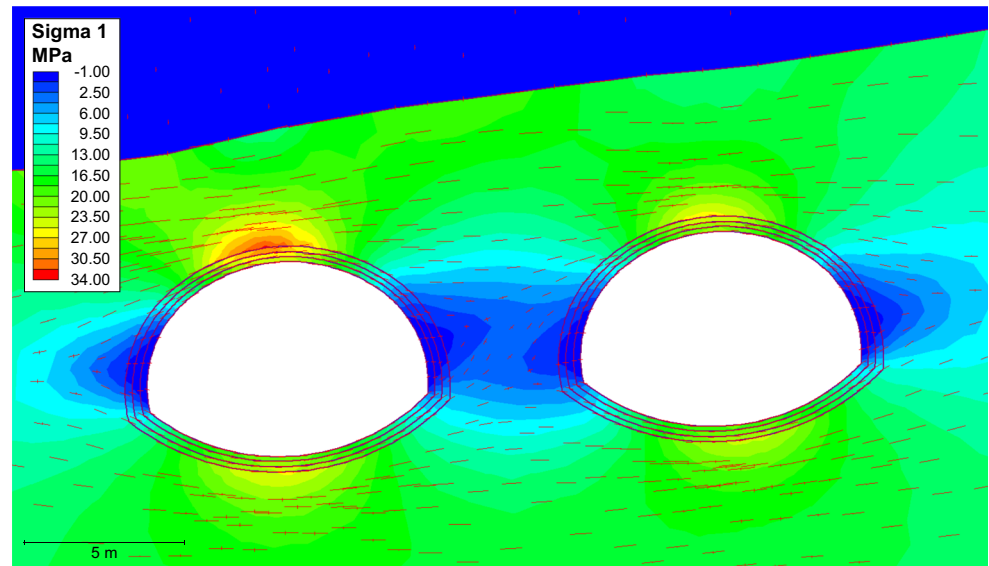
Actual support		Equivalent support	
RRS, c/c distance	2.5 m	Rebar spacing	0.4 m (Ø20 mm)
Rebar in RRS	6 x Ø20 mm	Rebar tensile strength	400 MPa
RRS thickness	0.3–0.5 m	Concrete thickness	0.3 m <sup>a</sup>
Sprayed concrete (smoothing layer)	0.18 m	Concrete compressive strength	40 MPa
Spiling bolts c/c dist.	0.3	Concrete E-modulus	25,000 MPa
Rock bolts	4 m (Ø20 mm) c/c 1.5 m	Rock bolts	4 m (Ø20 mm) c/c 1.5 m

measuring point by 1–1.5 tunnel diameters. Given this, the total deformation will be about 4 mm.

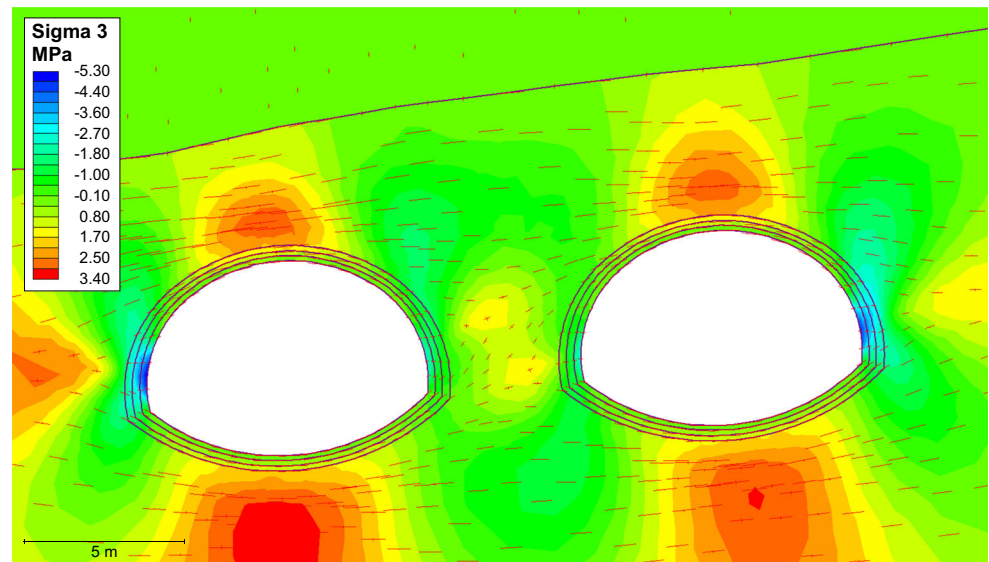
The rebar strain meters in the RRS showed quite low values. It is, therefore, difficult to determine whether the

registered strain is due to actual rock displacement or drying shrinkage in the concrete because the expected values for both are a few hundred µS. Some small impacts on the strain meters at B1028 may be related to the passing excavation of tube

**Fig. 17** Major principal stress with gravity-induced stress and an additional horizontal stress of 13.6 MPa



**Fig. 18** Minor principal stress with gravity-induced stress and an additional horizontal stress of 13.6 MPa



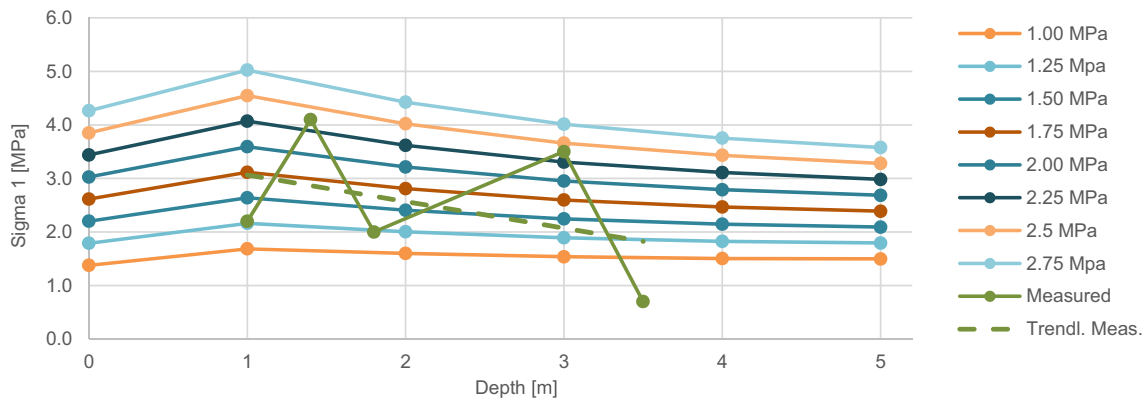


Fig. 19  $\sigma_1$  values from the roof in the model with various additional horizontal stresses

A. The readings of  $-250$  and  $-650 \mu\text{S}$  for left 1 and left 2 at B1220 (see Fig. 11) may also be related to the passing excavation of tube A.

The numerical modelling shows that the 3D stress measurements that were performed some distance away from the tunnel do not correspond well with the 2D stress

measurements performed close to the tunnel roof. If a rock mass with a high deformation modulus is near a rock mass with a lower deformation modulus, stresses will generally concentrate in the high deformation modulus rock mass. The syenite in the area has both a higher uniaxial compressive strength and a higher deformation modulus than the

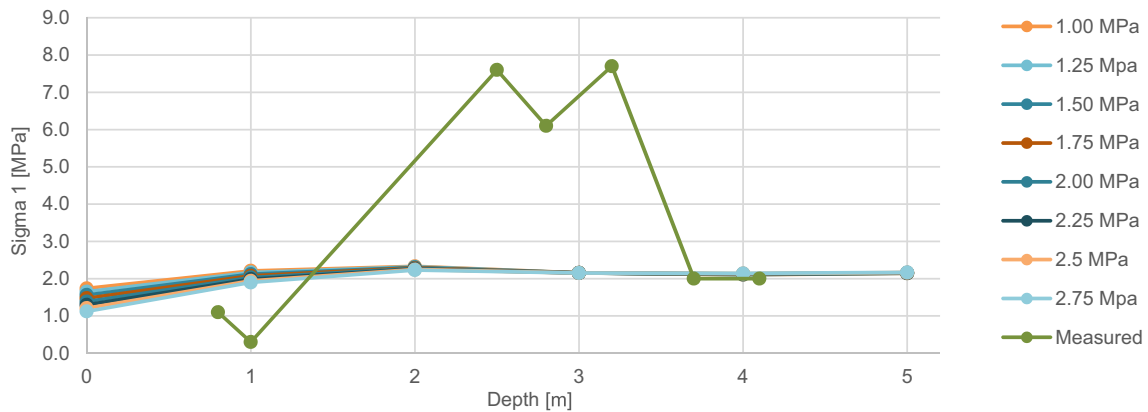
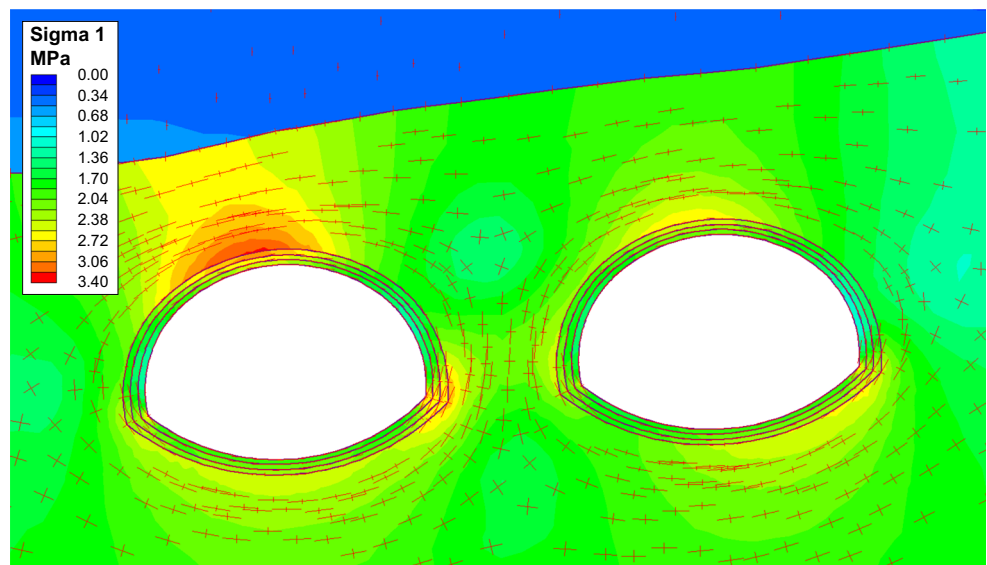
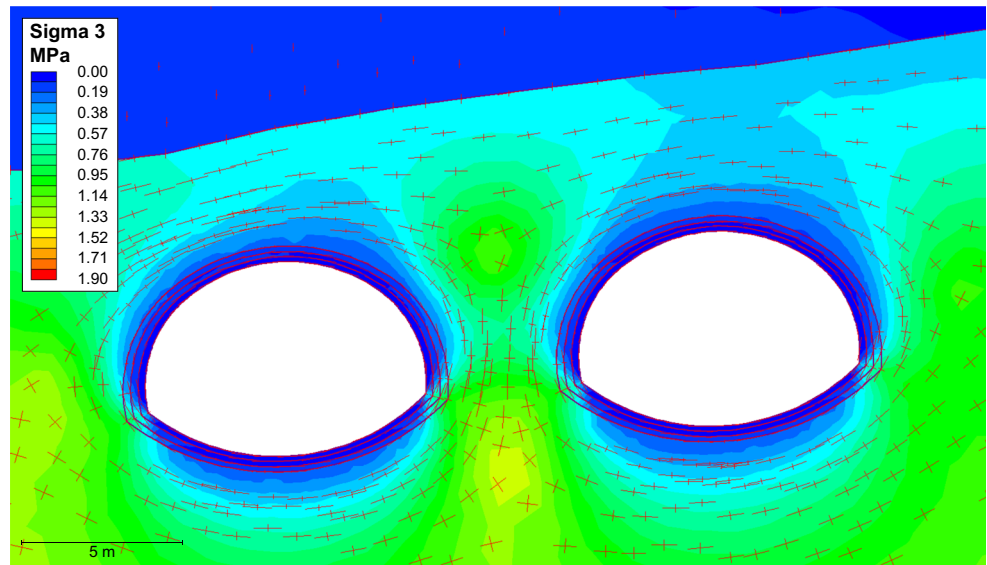


Fig. 20  $\sigma_1$  values from the pillar in the model with various additional horizontal stresses

Fig. 21 Major principal stress with gravity-induced stress and an additional horizontal stress of 1.50 MPa in the rock mass



**Fig. 22** Minor principal stress with gravity-induced stress and an additional horizontal stress of 1.50 MPa in the rock mass



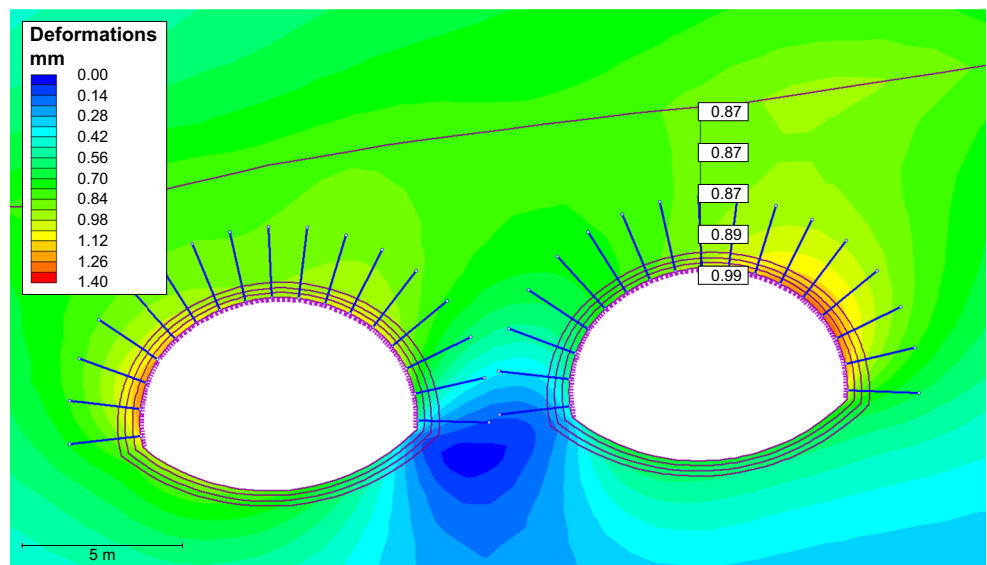
surrounding rock. The stress measurements have a quite large margin of error, which may be due to this change in deformation modulus, possible recordings in different rock types and joints being close to the individual measurements. In addition, the cooling of intrusive rock may create residual stresses. Because SC1 (see Fig. 17) has a  $\sigma_1$  of 20–25 MPa, the 2D measurements in the roof are of a different scale and there is a syenite intrusion in the area, it is likely that the 3D measurement has hit a local stress concentration. The quite high, negative, generally vertical minor principal stresses shown for SC1 in Fig. 18 are not likely occur in situ. This is because joints in the rock mass would release these stresses. The resulting stresses in the model from SC1 are considered implausible, and it is assumed that SC2, based on the 2D stress measurements, best fits the in-situ stresses. The negative sub-horizontal stresses in the pillar may be caused by the ability of

the rock to expand on two sides (normal to the  $\sigma_2$  direction), creating tension in the  $\sigma_2$  direction.

As shown by Fig. 19, the measured stresses do not follow the theoretical distribution, but have quite a considerable variation. This may be explained by the varying deformation modulus caused by the benching of the sandstone, local jointing and/or the local influence of high-pressure grouting. When considering the trend line in the same figure, it seems that the measured stress would match a field/additional horizontal stress of about 1.5 MPa. In this model, the total deformation in the roof is 1.18 mm and the relative deformation in the rock body is 0.16 mm, as compared to a deformation in the extensometer at B1220 of about 4 mm and a relative expansion between anchors 1 and 3 of 1.61 mm.

The rock overburden at B1220 is about 9 m and the measured relative deformation in excess of 1 mm can be

**Fig. 23** Deformations with gravity-induced stress and an additional horizontal stress of 1.50 MPa in the rock



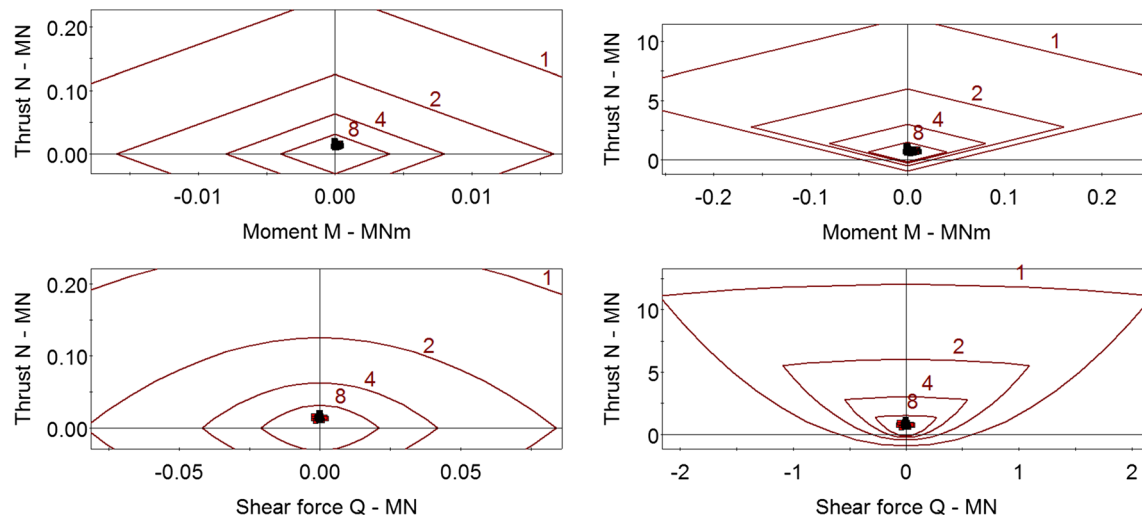


**Fig. 24** Capacity plot for the cast concrete simulating the ribs. The burgundy lines are the safety envelopes for safety factors 1, 2, 4 and 8

considered close to zero for practical purposes. This deformation may be caused by the displacement in a single joint and it is, therefore, not likely that a numerical model would yield the same deformation as the measured data when the deformations are this small.

Regarding the loading on the rib, a deformation in the rock of about 2–3 mm is expected after the mounting. This is because the rib is placed about 1 m behind the face and some of the deformation would already have taken place. The numerical model shows strains at the same level as those recorded by the strain meters but, as mentioned above, drying shrinkage may also cause strains at this level. The supposed strains in the rib from drying shrinkage and from deformations in the rock are moving in the same direction and it is difficult to distinguish which strains come from which sources. In either case, the numerical model shows very small loads on the support construction, far from its capacity (see Fig. 24), with millimetre-scale deformations.

There are several uncertainties and assumptions in the analyses presented in this paper, but the results are still quite unambiguous because the deformations are very small. Both the measurements and the modelling show that the ribs have little or no load. This means that the ribs do not have a support function, as they were designed to, but more of a rock-reinforcing function. It also indicates that the rock mass is self-bearing, provided that the contour is kept intact. Hoek and Marinos (2000) state that, in weak heterogeneous rock masses, sprayed concrete and bolting are sufficient rock reinforcements up to a tunnel closure of 1%. In this case, this means a deformation in the crown of about 6 cm.

The Q-values mapped during excavation in the area indicate a recommended rock support according to the Q-method very close to the border for where to start using RRS. Because of a long stretch with a low overburden and uncertain rock mass quality, spiling bolts and RRS were still chosen to be

used as an integrated part of the excavation process. The rock mass quality where one, according to the Q-method, should start to use RRS is based on empirical data. Considering the measured data, it seems that, with a rock mass quality at the border of requirement for RRS and probably also with quite worse rock mass, RRS is not required because of large stresses and deformations in the rock mass. The main function of the RRS is probably keeping the rock in place by locking blocks, increasing friction in the joints and preventing movement in larger filled joints. This goal can quite likely be obtained by an even leaner and more simply designed rib than the one used in this case.

**Open Access** This article is distributed under the terms of the Creative Commons Attribution 4.0 International License (<http://creativecommons.org/licenses/by/4.0/>), which permits unrestricted use, distribution, and reproduction in any medium, provided you give appropriate credit to the original author(s) and the source, provide a link to the Creative Commons license, and indicate if changes were made.

## References

- Aksoy CO, Ogul K, Topal I, Ozer SC, Ozacar V, Posluk E (2012) Numerical modeling of non-deformable support in swelling and squeezing rock. *Int J Rock Mech Min Sci* 52:61–70. <https://doi.org/10.1016/j.ijmms.2012.02.008>
- Barla G, Bonini M, Semeraro M (2011) Analysis of the behaviour of a yield-control support system in squeezing rock. *Tunn Undergr Space Technol* 26(1):146–154. <https://doi.org/10.1016/j.tust.2010.08.001>
- Carranza-Torres C, Diederichs M (2009) Mechanical analysis of circular liners with particular reference to composite supports. For example, liners consisting of shotcrete and steel sets. *Tunn Undergr Space Technol* 24(5):506–532. <https://doi.org/10.1016/j.tust.2009.02.001>
- Gilbert RI (2001) Shrinkage, cracking and deflection—the serviceability of concrete structures. *Electron J Struct Eng* 1(1):15–37



- Grimstad E, Kankes K, Bhasin R, Magnussen AW, Kaynia AM (2002) Rock mass quality Q used in designing reinforced ribs of sprayed concrete and energy absorption. *Fjellsprengningsteknikk—bergmekanikk—geoteknikk*, Oslo, November 21–22, 2008
- Grimstad E, Tunbridge L, Bhasin R, Aarset A (2008) Measurements of deformation and forces in reinforced ribs of sprayed concrete. Why do we use cast concrete lining when ribs of sprayed concrete have a large margin? *Fjellsprengningsteknikk—bergmekanikk—geoteknikk*, Oslo, November 20–21, 2008
- Hoek E (1998) Tunnel support in weak rock. *Symposium of Sedimentary Rock Engineering*, Taipei, Taiwan, November 20–22, 1998
- Hoek E, Diederichs MS (2006) Empirical estimation of rock mass modulus. *Int J Rock Mech Min Sci* 43(2):203–215. <https://doi.org/10.1016/j.ijrmmms.2005.06.005>
- Hoek E, Marinov P (2000) Predicting tunnel squeezing problems in weak heterogeneous rock masses. *Tunnels Tunn Int* 32(11):45–51
- Hoek E, Kaiser PK, Bawden WF (1997) Support of underground excavations in hard rock, 3rd edn. Balkema, Rotterdam
- Hoek E, Carter TG, Diederichs MS (2013) Quantification of the geological strength index chart. 47th US Rock Mechanics/Geomechanics Symposium, San Francisco, June 23–26, 2013
- Høien AH, Nilsen B (2014) Rock mass grouting in the Løren tunnel: case study with the main focus on the groutability and feasibility of drill parameter interpretation. *Rock Mech Rock Eng* 47(3):967–983. <https://doi.org/10.1007/s00603-013-0386-7>
- Humstad T, Høien AH, Kveen A, Hoel JE (2012) Complete software overview of rock mass and support in Norwegian Road Tunnels, Eurock 2012. ISRM, Stockholm, Sweden.
- International Society for Rock Mechanics (ISRM) (2007) The complete ISRM suggested methods for rock characterization, testing and monitoring: 1974–2006. ISRM Turkish National Group, Ankara
- Iversen E (2011) Lørentunnelen - Longitudinal general geology section map
- Iversen E, Kveen AT (2007) Rv. 150, Lørentunnelen, Geologisk rapport for konkurransegrunnlaget, Oppdrag A-37A, rapport nr. 3. Statens Vegvesen, Oslo
- Kim K, Franklin JA (1987) Suggested methods for rock stress determination. *Int J Rock Mech Min Sci Geomech Abstr* 24(1):53–73
- Larsen T (2010) 3-dimensjonal og 2-dimensjonal bergspenningsmålinger ved Lørentunnelen. SINTEF, Trondheim
- Larsen T, Trinh NQ (2014) In-situ rock stress measurements and numerical modelling. SINTEF, Trondheim
- Mao DW, Nilsen B, Lu M (2011) Analysis of loading effects on reinforced shotcrete ribs caused by weakness zone containing swelling clay. *Tunn Undergr Space Technol* 26(3):472–480. <https://doi.org/10.1016/j.tust.2011.01.004>
- Myrvang A (2001) Bergmekanikk. Department of Geology and Mineral Resources Engineering, NTNU, Trondheim
- Norsk Forening for Fjellsprengningsteknikk (NFF) (2008) Tung bergsikring i undergrunnsanlegg, vol 5. Håndbok. NFF, Oslo
- Norwegian Geotechnical Institute (NGI) (2013) Using the Q-system—rock mass classification and support design. Handbook. NGI, Oslo
- Oftedal C (1981) Norges geologi/geology of Norway. Tapir, Trondheim
- Pedersen KB, Kompen R, Kveen A (2010) Arbeider foran stoff og stabilitetssikring i vegtunneler. Teknologirapport. Norwegian Public Roads Administration, Oslo
- Rocscience Inc. (2015) RocData, vol 5.006. Rocscience Inc., Toronto
- Rocscience Inc. (2016) RS2, vol 9.011. Rocscience Inc., Toronto
- Schwingschloegl R, Lehmann C (2009) Swelling rock behaviour in a tunnel: NATM-support vs. Q-support—a comparison. *Tunn Undergr Space Technol* 24(3):356–362. <https://doi.org/10.1016/j.tust.2008.08.007>
- Sjöberg J, Klasson H (2003) Stress measurements in deep boreholes using the Borre (SSPB) probe. *Int J Rock Mech Min Sci* 40(7–8): 1205–1223. [https://doi.org/10.1016/S1365-1609\(03\)00115-1](https://doi.org/10.1016/S1365-1609(03)00115-1)
- Standard Norge (2008) Eurocode 2: design of concrete structures. Part 1-1: general rules and rules for buildings. Standard Norge, Lysaker
- Vianova Systems (2011) Novapoint Tunnel, 18th edn. Vianova Systems, Sandvika